Breeze effects at a large artificial lake: summer case study

Maksim Iakunin[1], Rui Salgado[1], and Miguel Potes[1]

[1]Department of Physics, ICT, Institute of Earth Sciences, University of Évora, 7000 Évora, Portugal

Correspondence to: Maksim Iakunin (miakunin@uevora.pt)

Abstract. Natural lakes and big artificial reservoirs can affect the weather regime of surrounding areas but, usually, consideration of all aspects of this impact and their quantification is a difficult task. Alqueva reservoir, the largest artificial lake in Western Europe located on the southeast of Portugal, was filled in 2004. This makes it a large laboratory and allows to study the changes in the surface and in the landscape and how they affect the weather in the region. This paper is focused on a case study of a 3 days intensive observation period of 22-24 July 2014. In order to quantify the breeze effects induced by Alqueva reservoir, two simulations with the mesoscale atmospheric model Meso-NH coupled to FLake freshwater lake model has been done. The principal difference of these two simulations is in the presence of the reservoir in the input surface data. Comparing two simulations datasets: with and without the reservoir, net results of the lake impact were obtained. Magnitude of the impact on the air temperature, relative humidity, and other atmospheric variables is shown. Clear effect of a lake breeze (5-7 m/s) can be observed during the daytime on the distances up to 6 km away from the shores and up to 300 m over the lake surface. Lake breeze system starts to form at 9:00 UTC and dissipates at 18:00-19:00 UTC with the arrival of a larger scale Atlantic breeze. The descending branch of the lake breeze circulation brings dry air from higher atmospheric layers (2-2.5 km) and redistributes it over the lake. It is also shown that despite its significant intensity the effect is limited to a couple of kilometers away from the lake borders.

1 Introduction

Human activities, such as urbanization, deforestation or water reservoirs building change the properties of the surface (vegetation cover, emissivity, albedo) which rule the surface energy fluxes (Cotton and Pielke, 2007). As a consequence, changes in surface energy fluxes affect local weather and climate. Lakes and reservoirs contains about 0.35% of global freshwater storage (Hartmann, 1994) and cover only 2% of continental surface area (Segal et al., 1997). Thermal circulations triggered by lake/land thermal contrast have an impact on dispersion of air pollution and lake catchment transport (Lee et al., 2014). Big lakes being a significant source of atmospheric moisture can intensify storm formation (Samuelsson et al., 2006; Zhao et al., 2012). Lakes and reservoirs, compared to land surfaces, have higher thermal inertia and heat capacity, and lower albedo and roughness length (Bonan, 1995). They can affect meteorological conditions and atmospheric processes at meso and synoptic scales (Pielke, 1974; Bates et al., 1993; Pielke, 2013).

Normally, near surface relative humidity is increased while daily air temperature is decreased above lake and shore areas. During the warm summer periods relatively colder lake surface interacts with the atmosphere above, which leads to a

reduction of clouds and precipitation. Formation of the local high pressure areas over the lake surface in summer season supports atmospheric circulation, which can be observed as a lake breeze (Bates et al., 1993). In autumn and winter it has the opposite effect: due to the fact that water is warmer than the air above, increase of evaporation and cloud formation can be observed (Ekhtiari et al., 2017). These regional lake effects have been seen in previous studies, e.g. Elqui Valley reservoir in

5 Chile (Bischoff-Gauß et al., 2006) and the great African lakes (Thiery et al., 2014).

Although the theoretical aspects of formation of the lake breezes are clear, in practice, they remain not well documented. Difficulties in studies of lake breeze are due to the diversity and complexity of lake shapes and surrounding landscapes, and the inexistence of observational data at sufficiently fine spatial resolution (Segal et al., 1997).

Lake breezes are mainly determined by the landscape and weather conditions. Formation and intensity of the breeze depend
10 on the set of parameters such as large scale winds, sensible heat flux, geometry of the lake and terrain types of the surrounding area (Segal et al., 1997; Drobinski and Dubos, 2009; Crosman and Horel, 2012).

In this work, the focus is on the study of the lake breeze at the Alqueva reservoir and its impact on atmospheric parameters of the surrounding area. This large artificial reservoir has been filled in 2004 which makes it a big natural laboratory for studying physical, chemical, and biological effects. Few studies about the influence of Alqueva on atmosphere and climate
15 were published. The first report, in Portuguese, was published even before the construction of the dam by Miranda et al. (1995), as a part of the environmental impact study of the reservoir on the basis of numerical simulations performed with the NH3D (non-hydrostatic 3-dimensional) mesoscale model from Miranda and James (1992). It was concluded that the climate impact of the multi-purpose Alqueva project should be merely due to the irrigation of surrounding area. The influence of the reservoir itself was unclear as at that time it was not possible to perform high resolution simulations. The studies were
20 continued and improved by Salgado (2006) who did the first attempt to quantify the direct effect of the reservoir on the local climate, in particular on winter fog. Using the Meso-NH (non-hydrostatic mesoscale atmospheric model) model, the author concluded that the introduction of the reservoir should increase slightly the winter fog in the surrounding area, but decrease over the filled area. Later on, Policarpo et al. (2017), used observations data from two periods of ten years (before and after Alqueva reservoir) combined with Meso-NH simulations, and showed a slight increase in the average number of days with fog
25 during the winter (about 4 days per winter after 2003 in a downwind site).

Mesoscale atmospheric models, such as Meso-NH, allow to obtain results with sufficient horizontal resolution (250 m in present study) for studying the local effects of air temperature changes and the generation of small-scale circulations under different large-scale atmospheric situations. In this work simulations have been done for the Intensive Observation Period (IOP) of ALEX project (ALqueva hydro-meteorological EXperiment, http://www.alex2014.cge.uevora.pt/). Data collected during
30 this experiment were used to validate the numerical simulations.

The article outline is the following. Section 2 provides a brief description of the Alqueva reservoir. Section 3 reveals information about ALEX experiment and the measurement data used in this paper such as meteorological stations, observations, and measurements. Section 4 contains a brief description of the numerical models used in this work: Meso-NH and FLake. Sections 5 and 6 are dedicated to the case study on 22-24 July 2014: validation of simulation results using in-situ measurements
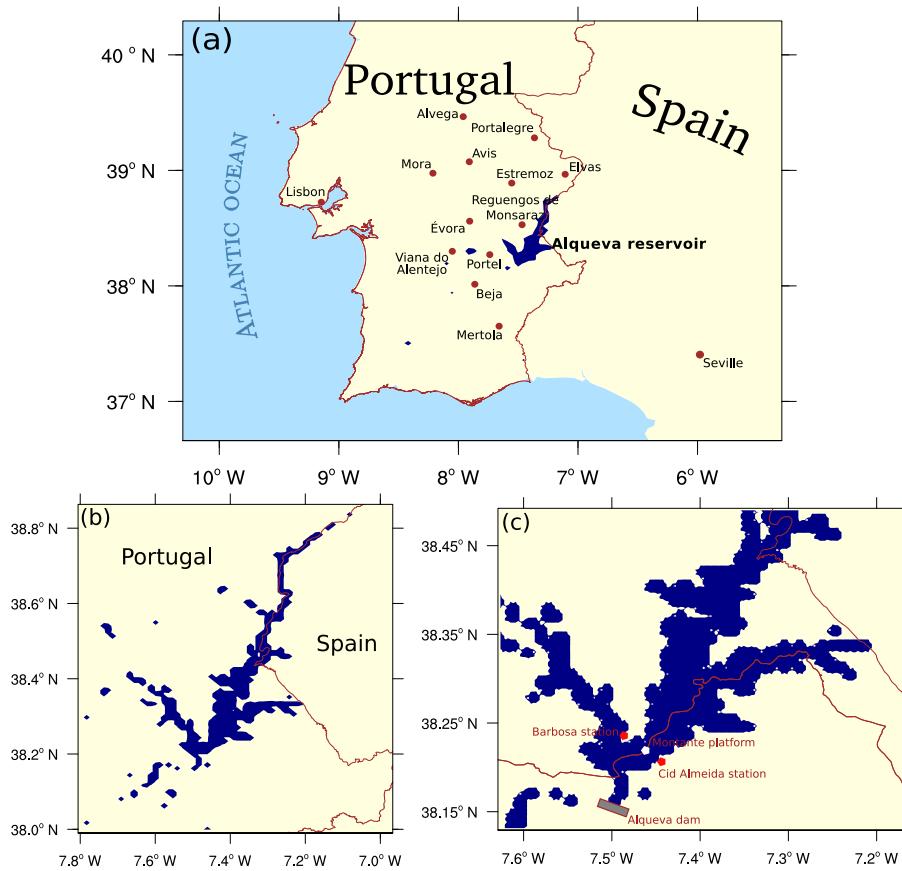
Figure 1. Nested domains used in the simulations: **(a)** Father domain at 4 km horizontal resolution with 100×108 grid points, with location of the 12 IPMA synoptic stations used for validation, **(b)** intermediate 1 km horizontal resolution domain, 96×72 grid points, **(c)** finer 250 m resolution domain comprising 160×160 grid points, together with the location of the ALEX land stations, the Montante floating platform and the dam.

and the studies of the lake effects respectively, with an illustration and discussion of the magnitude of the impact and intensity of a lake breeze. Section 7 summarizes the results and conclusions.

2   Object of study

Alqueva reservoir established in 2002 is an artificial lake located in the southeast part of Portugal. It spreads along 83 km over
5   the Guadiana river valley covering, when completely filled, an area of 250 km^2 with a capacity of 4.15 km^3, which makes it the largest artificial lake in Western Europe (Fig. 1 (a)). The maximum and average depths of the reservoir are 92 m and 16.6 m respectively. The dam is located in the southern part of the reservoir (Fig 1 (c)).

Alqueva reservoir is mainly used to provide water supply, irrigation, and hydroelectric power. The region where it is located is known for the irregularity of its hydrological resources, with long periods of drought that could last for more than one consecutive year (Silva et al., 2014). This region has an Mediterranean climate with dry and hot summers (Csa according to the Köppen climate classification), with a small area within of the mid-latitude steppe (BSk) category. During summer, the

5   maximum air temperature ranges between 31 and 35 °C on average (July and August), often reaching values close to 40 °C, or even higher. The incident solar radiation at the surface is of the highest in Europe, with mean daily values (integrated over 24 hours) of about 300 Wm^{-2} and the daily maximum of July often can reach 1000 Wm^{-2}. Rainfall periods are seasonal and last from October to April. The normal (1981-2010) average annual precipitation in the city of Beja (40 km from Alqueva reservoir) is 558 mm (www.ipma.pt).

10   Two major factors determine synoptic circulations over the region during the summer period: the shape and location of the Azores anticyclone, and the frequent establishment of a low-pressure system over the Iberian Peninsula, induced by the land-ocean thermal contrasts. The sea breeze system controls the transport of the maritime air masses from the Atlantic to Iberian Peninsula, on distances more than 100 km reaching the Alqueva region in the late afternoon. This phenomenon is known as the Iberian thermal low (Hoinka and Castro, 2003) and is characterized by a westward change of the wind direction (prevailing

15   wind directions are from the northwest quadrant). As a result, this effect is observed in the local increase in wind intensity and in its rotation (Salgado et al., 2015).

3   Measurement data

The measured data used in this work were obtained during the ALEX campaign — a multidisciplinary observational experiment at the Alqueva reservoir which lasted from June to October 2014. One of the aims of this project was to perform a wide set

20   of measurements of chemical, physical, and biological parameters in the water, air columns, and over the water-atmosphere interface. To reach this goal the project operated the following facilities:

- 7 sites with meteorological measurements: 2 platforms (Montante and Mourão); 1 permanent weather station located in a small island nearby the dam (Alquilha), 2 dedicated weather stations (Barbosa and Cid Almeida), two compact weather stations in the Solar Park and Amieira;

25   - 4 floating platforms where water quality and biological sampling were done: Montante, Mourão, Captação, and Alcarrache;

- 3 weather stations of Instituto de Ciências da Terra (ICT), located in Mitra, Portel, and at the University of Évora;

- 2 Air quality mobile units: Amieira and Solar Park;

- 3 Atmospheric Electricity stations: Amieira, Solar Park, and Beja.

Also, data from 42 IPMA (Portuguese Institue of Sea and Atmosphere) meteorological stations located in the region were integrated into ALEX database. They provided typical set of variables, e.g. air temperature, relative humidity, pressure, horizontal wind speed.

Two land weather stations (Barbosa and Cid Almeida) were installed on opposite shores (38.2235° N, 7.4595° W and 38.2164° N, 7.4545° W, correspondingly) while the floating platform Montante is situated in the middle (38.2276° N, 7.4708° W, Fig. 1 (c)). This locations allowed the characterization of the lake effects ion a fine scale. Land stations collected data with an 1-minute time resolution including horizontal wind speed, relative humidity, air temperature, and downwelling short-wave radiation. Montante floating platform was the principal experimental site inside the reservoir. The following equipment was installed there on 2 June 2014 and data has been collected until the end of the campaign:

– an eddy-covariance system which provides data for pressure, temperature, water vapor and carbon dioxide concentrations, 3D wind components, momentum flux, sensible and latent heat fluxes (with 30 minutes timestep), carbon dioxide flux, evaporation;

– one albedometer and one pirradiometer in order to measure upwelling and downwelling shortwave and total radiative fluxes;

– 9 thermistors to measure water temperature profile.

The intensive observation period of the ALEX project lasted 3 days (22-24 July) and included launches of meteorological balloons every 3 hours. In total, 18 radiosondes were launched: 2 from the boat over the lake and 16 from the land. Atmospheric profiles of air temperature, relative humidity, wind, and pressure were obtained. This period, 22-24 July, was chosen for a case study in the this work,as it is an well documented period with typical anticyclonic conditions, hot, dry and low near surface wind speed.

Data collected during the ALEX field campaign have already been used to study: lake-atmosphere interactions, including the heat and mass (H_2O and CO_2) fluxes in the interface water-air (Potes et al., 2017); the effects of inland water bodies on the atmospheric electrical field (Lopes et al., 2016); and the evolution of the vertical electrical charge profiles and its relation with the boundary layer transport of moisture, momentum and particulate matter (Nicoll et al., 2018).

4 Simulation setup

4.1 Meso-NH atmospheric model

To study the lake breeze effects in Alqueva reservoir the Meso-NH model (Lac et al., 2018) was used. Meso-NH is a non-hydrostatic mesoscale atmospheric research model. It can simulate the evolution of the atmosphere on scales ranging from large (synoptic) to small (large eddy), and has a complete set of physical parametrizations. Meso-NH is coupled with SURFEX (Surface Externalisée, Masson et al. (2013)) platform of models for the representation of surface-atmosphere interactions by considering different surface types (vegetation, city, ocean, inland waters).

Meso-NH allows a multi-scale approach through a grid-nesting technique (Stein et al., 2000). In this work, three nesting domains were used: $400 \times 432 \text{ km}^2$ domain with 4 km horizontal resolution to take into account the large scale circulations, namely the influence of the sea breeze (Fig. 1 (a)), an intermediate $96 \times 72 \text{ km}^2$ domain with 1 km horizontal resolution centered at the Alqueva reservoir (Fig. 1 (b)), and a finer $40 \times 40 \text{ km}^2$ domain with 250 m spatial resolution to track the small scale effects of the lake (Fig. 1 (c)). Hereinafter we denote this three domains A, B, and C correspondingly. The two-way nesting technique used in Meso-NH allows to conduct simulations on different horizontal resolutions at the same time. Domain A is a "father" domain for B, which means that simulation results on domain A are interpolated and used as initial and boundary conditions for domain B. Same scheme applies for domains B/C. European Centre for Medium-Range Weather Forecast (ECMWF) operational analyses, updated every six hours, were used for Meso-NH initialization and domain A boundary forcing.

For surface and orography, ECOCLIMAP II (Faroux et al., 2013) and SRTM (Shuttle Radar Topography Mission, Jarvis et al. (2008)) databases were used, respectively, both updated with the inclusion of Alqueva reservoir by Policarpo et al. (2017). All model domains had 68 vertical levels starting with 20 m and up to 22 km, including 36 levels for the lower atmospheric level (2 km). The model configuration included a turbulent scheme based on a one-dimensional 1.5 closure (Bougeault and Lacarrere, 1989). A mixed-phase microphysical scheme for stratiform clouds and explicit precipitation (Cohard and Pinty, 2000; Cuxart et al., 2000) which distinguishes six classes of hydrometeors (water vapor, cloud water droplets, liquid water, ice, snow, and graupel) was used. Longwave and shortwave radiative transfer equations are solved for independent air columns (Fouquart and Bonnel, 1980; Morcrette, 1991). Atmosphere-surface exchanges are taken into account through physical parametrizations: the surface soil and vegetation are described by the Interface Soil Biosphere Atmosphere (ISBA) model (Noilhan and Mahfouf, 1996); the town energy balance was handled according to Masson (2000). Basic parameters for each model domain are shown in the Table 1. Deep and shallow convection parametrization schemes were activated in the coarser domain A. 1-km and 250-m resolutions of domains B and C are high enough for the deep/shallow convection to be represented explicitly. The following schemes were used (see Table 1): KAFR (Kain and Fritsch, 1990; Bechtold et al., 2001), EDKF (Pergaud et al., 2009), WENO (Lunet et al., 2017), and ICE3 (Pinty and Jabouille, 1998).

To track the impact of the reservoir on the weather conditions, two numerical simulation were performed: one with the surface input files updated to include the Alqueva reservoir (ECOCLIMAP database version updated by Policarpo et al., 2017) and another with the previous version of this database where the reservoir does not exist yet. In order to distinguish these simulations hereinafter we denote them LAKE1 and LAKE0, correspondingly. Both simulations covered the case study period, 22-24 July 2014, with 1 hour output. To reproduce the atmospheric conditions more realistically the simulations included the previous 24 hours (21 July), so the model was integrated for 96 hours. The differences between these two simulations were then computed, with the aim of evaluating the direct influence of the lake on the atmosphere.

4.2 FLake model

In order to better represent the evolution of the lake surface temperature and therefore the water-air heat fluxes, FLake (Freshwater Lake) model (Mironov, 2008) was used. FLake is a bulk-type model capable to predict the evolution of the lake water temperature at different depth on time scales from a few hours to many years. For an unfrozen lake it uses a two-layer ap-

Table 1. Summary of the Meso-NH physical schemes used in the simulations.

Schemes and parameters	Domains		
	A	B	C
Deep convection	KAFR	NONE	NONE
Shallow convection	EDKF	EDKF	NONE
Turbulence	BL89	DEAR	DEAR
	1 dimension	3 dimensions	3 dimensions
Radiation transfer	ECMW	ECMW	ECMW
Advection	WENO	WENO	WENO
Clouds	ICE3	ICE3	ICE3
Timestep	20 s	5 s	1 s

proach: upper mixing layer with a constant water temperature and the thermocline beneath it where the temperature decreases with depth. Parametrization of the thermocline profile is based on the concept of self-similarity assuming that such approach could be applied to all natural and artificial freshwater lakes.

FLake model requires at least the following sets of variables and parameters to run: four initial parameters to describe the lake temperature structure, six atmospheric input variables for each timestep, and two parameters — lake depth and the attenuation coefficient of light in the water. This coefficient is used to compute the penetration of the solar radiation in the water body. In this work, the attenuation coefficient was set to 0.85 based on in-situ measurements carried out in Alqueva by Potes et al. (2017).

The FLake prognostic variables that need to be initialized are: water temperature at the bottom, temperature and depth of the mixing layer, and shape factor C_f — a parameter that describes the shape of the the thermocline curve. In the parametrization proposed by Mironov (2008) for the normalized temperature profile it varies from 0.5 to 0.8. The initial values of the shape factor C_f, a water mixing layer temperature, and depth were determined using a fitting technique applied to the observed water temperature profile at a given time in Montante platform (Fig. 2 (a)). Short term FLake model runs are very sensitive to initial parameters. The fitting technique is based on the assumption that the bottom temperature is fixed and given by the value of the lowermost sensor. Thereby, the other three parameters could vary within some range until the best set is found. The initial conditions for our simulations were obtained following this technique: $C_f = 0.8$, mixed layer temperature is 23.8 °C and depth is 3.4 m. Test simulation with these set of inputs was done using stand-alone version of FLake model (not in couple with Meso-NH). The results of the comparison of water mixing layer temperature is shown in Fig. 2 (b). The maximum difference does not exceed 0.8 °C which is a very good result for such short-term simulation.
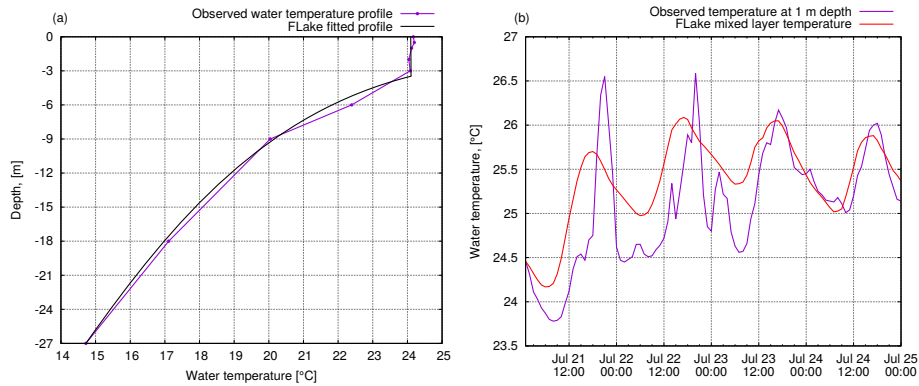
Figure 2. Water temperature observed and fitted profiles on July 21, 00:00 at the Montante platform (a) and comparison of upper level water temperature between measurements and FLake results (b)

The observed daytime temperature profiles showed strong skin effects (higher temperatures in first 10 cm) and could not be well fitted by a FLake type temperature profile, which assumes a constant temperature in the mixed layer. Thus, the midnight profile was used as an initial one and the simulation started at midnight, 21 July 2014.

The required atmospheric variables were taken interactively from Meso-NH simulation since FLake was implemented in
5   SURFEX model by Salgado and Le Moigne (2010).

The depth of the artificial lakes varies decreases rapidly from the center to the shore, because the bottom of the reservoirs used to be valleys. In case of Alqueva, when completely filled, the mean depth is of about 17 m (http://www.edia.pt/). On the other hand, the local depth at Montante platform can reach 70 m. As an 1D bulk model, FLake has only one depth value which should be seen as an effective depth and is not easy to assess. Moreover, FLake model is not capable to represent deep lakes, it
10   works well for depths from 20 to 50 m with the sediments routine switched-off. After a series of a sensitivity tests of short-term (2-4 days) and long-term (2-4 months) simulation it was found that the best simulations results can be obtained with the bottom depth value of 20-30 m. Thus, since the deepest temperature probe was installed at the depth of 27 m, this value was chosen for the effective lake depth in this work. The comparison between measurements of water temperature near surface (at 1 meter depth) and FLake simulated values of mixed layer temperature are shown in Fig. 2 (b). Sensor at 1 meter depth was chosen
15   because it always stays in mixed layer and is not affected by surface "skin" effects. Modelled values are close to measurements which indicates that the initial conditions were realistically imposed.

5 Validation

The simulation LAKE1 results were validated against radiosondes data (vertical profiles) and meteorological data from ALEX and IPMA stations located on land and in the floating platforms. All three domains were considered in the validation. The size
20   of the domain A was enough to consider 12 synoptic stations located in the region, domain B was used to track the radiosondes
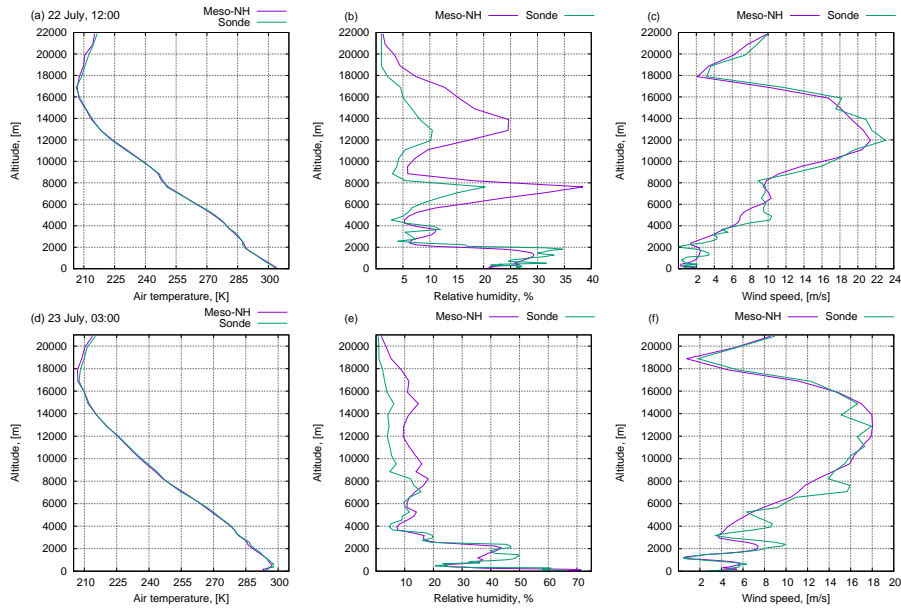
Figure 3. Examples of observed and simulated vertical profiles for July 22, 12:00 and July 23, 3:00 of air temperature (a, d), relative humidity (b, e), and wind speed (c, f).

trajectory, and domain C results were validated against stations installed on the lake shores and on the Montante floating platform. The variables under analysis were air temperature, relative humidity, wind speed, sensible and latent heat fluxes.

5.1   Comparison with radiosondes data

The ALEX IOP took place between 22 and 24 of July 2014 at the Alqueva reservoir. It included the launch of 18 meteoro-
5   logical balloon every 3 hours. The radiosondes took measurements of air temperature, humidity, pressure, and wind speed. As the balloons did not ascent vertically and flew several kilometers away from the launching point, a trajectory profile compar-ison was performed. Each balloon had a GPS-tracker to register its coordinates every 2 seconds, which was used to build a corresponding numerical trajectory on the simulation domain. Radiosondes reached the altitude of the top of the model (about 22 km) in about 2.5 hours. Therefore in order to build the simulated profile, three consecutive hourly outputs from the model
10   were used.

Figures 3 (a, b, c) represent examples of the daytime profiles of air temperature, relative humidity, and horizontal wind speed. Examples of night profiles can be found in figures 3 (d, e, f). In general, the night simulated profiles show slightly better accordance with model results.

Figure 4 shows the same profiles, but for the lower troposphere level (3000 m altitude). Simulation are in good accordance
15   with observations. The simulation results are within the confidence interval of the measurements as given by the radiosonde accuracy ($\pm0.5°$C, $\pm5\%$ relative humidity, and ±0.15 m/s wind speed with 2-sigma confidence level (95.5%)).
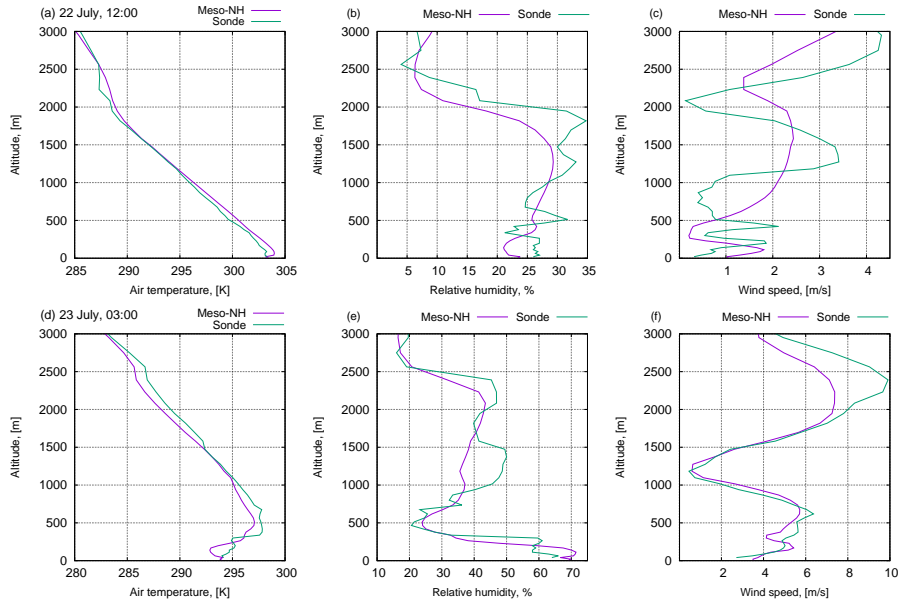
Figure 4. Profiles of air temperature, relative humidity, and wind speed in low atmosphere on 22 July 12:00 and 23 July 03:00.

The principal features of the profiles trend are well represented by the model. During daytime, air temperature and relative humidity curves indicate that the model tends to well represent the height of the boundary layer at 2-2.5 km altitude (around 2 km in Fig. 4 (a), (b)). Overall, Meso-NH reproduces the air temperature above the surface layer (over 500 m) very well. Near surface, the Meso-NH tends to anticipate the development of the unstable boundary layer in the morning (9:00 and 12:00

5   UTC), simulating higher temperatures in the lower levels. In the late afternoon (18:00 and 21:00 UTC) the model also tends to anticipate the decrease of the temperature in the surface layer (see the supplementary material, Fig. S1).

The patterns of relative humidity and wind speed are good, as observed and modelled curves look similar, nevertheless simulations tend to be more conservative and their values do not change so quick. Nocturnal low level jets at the edge of the boundary layer are represented by the model, but their magnitude is slightly weaker than the observed. All the profiles can be

10   found in the supplementary material (Fig. S3). The moisture vertical profile in the boundary layer is well reproduced by the model, as can be seen in the graphs of the relative humidity (Fig. 4 (b), (e), and S2 in the supplementary materials). Above the boundary layer the radiosondes show a dry layer, which is also well simulated. From July 23 the observations show the appearance of a moist layer close to the troposphere, which magnitude is overestimated by the model. On July 24 at dawn the radiosondes and the model indicate the existence of a very moist layer close to the surface, with the formation of low clouds

15   that were not formed in the simulations.

Statistical results for them are the following: temperature average bias is -0.13 °C, RMSE is 1.49 °C, and correlation coefficient is 0.99; relative humidity average bias is 0.59%, RMSE is 11.26%, and correlation coefficient is 0.87; and for the wind speed average bias is 0.05 m/s, RMSE is 2.07 m/s, and correlation coefficient is 0.90. These values testify that the
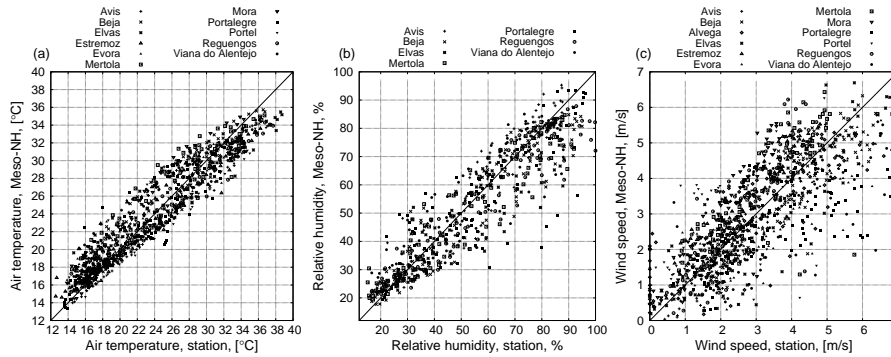
Figure 5. Scatter plots of the comparison between Meso-NH sumulation LAKE1 and measured values at synoptic stations. Air temperature **(a)**, relative humidity **(b)**, and horizontal wind speed **(c)**.

simulation is in a good accord with the observations, in line with similar studies of Meso-NH validation against radiosondes data (e.g., Masciadri et al., 2013).

5.2 Comparison with IPMA stations data

The model was also validated against 12 IPMA automatic meteorological stations. For this comparison the output of the bigger
5   domain A were used. Geographical positions of the stations can be found in Fig. 1 (a). Scatter plots of air temperature, relative humidity, and wind speed are shown in Fig. 5. It should be mentioned that not all stations provided the same set of variables. The scatter plots show the intercomparison of the model data (X axis) and the measured values (Y axis) over all the simulated period and all the stations. The model tends to overestimate lower values of air temperature (14-24 °C) and slightly underestimate higher values (>30 °C), as can be seen from Fig. 5 (a). Over some stations and in several times, the model simulates lower
10   values of relative humidity within the range from 40 to 100% (Fig. 5 (b)). Fig. 5 (c) indicates that the wind speed is slightly underestimated by the model.

Statistical parameters (bias, mean absolute error, root mean squar, and correlation coefficient) for each station are shown in Table 2. Simulated and observed air temperature are highly correlated (correlation coefficient is higher that 0.91) with bias always less than 1 degree. The worst results are observed in Portalegre (square points in relative humidity plot in Fig. 5 (b)),
15   and a possible reason for this relies on the location of the station which is installed in small mountain area. Regarding the wind speed, Table 2 shows small biases, in general lower than 1 m/s, and relatively high correlation coefficients for wind simulations (0.68 - 0.92). The lowest correlation coefficient is also obtained in Portalegre. Overall, simulation results are in good agreement with synoptic stations data, and the statistical parameters are similar to other published works done with Meso-NH (e.g., Lascaux et al., 2013, 2015).

Table 2. Statistics for the hourly values of the station validation.

Stations:		Alvega	Avis	Beja	Elvas	Estrem.	Évora	Mert.	Mora	Portal.	Portel	Reguen.	V. Alen.
Temp.,	Bias:	—	-0.08	0.68	-0.39	0.00	0.56	0.85	0.9	-0.08	-0.30	-0.33	0.52
°C	MAE:	—	1.49	1.60	1.76	1.65	1.60	1.71	1.54	1.82	1.91	1.44	1.82
	RMS:	—	1.84	1.96	2.18	2.02	1.96	2.20	1.93	2.38	2.27	1.82	2.13
	Corr:	—	0.95	0.96	0.96	0.96	0.96	0.95	0.96	0.91	0.94	0.97	0.96
Rel.	Bias:	—	0.53	-2.98	-3.42	—	—	-1.29	-4.19	-2.79	—	-4.10	1.80
hum.,	MAE:	—	5.80	7.48	5.87	—	—	6.61	6.88	7.83	—	6.94	8.08
%	RMS:	—	7.41	9.49	8.61	—	—	8.49	8.43	11.91	—	9.11	9.80
	Corr:	—	0.93	0.93	0.93	—	—	0.94	0.94	0.86	—	0.95	0.90
Wind	Bias:	-0.46	-0.34	-0.16	-0.09	-0.91	0.27	-1.11	-1.09	0.53	-0.78	-0.86	0.18
speed,	MAE:	2.33	0.26	0.22	0.88	1.28	0.44	0.74	1.19	0.68	1.02	0.32	0.43
m/s	RMS:	1.01	0.73	0.74	1.01	0.69	0.94	0.93	0.93	1.12	1.16	1.03	1.19
	Corr:	0.85	0.92	0.91	0.86	0.92	0.82	0.81	0.85	0.68	0.69	0.86	0.71

5.3 Comparison with data from ALEX database

In addition to the validation against the IPMA synoptic stations, comparisons were made with data obtained at ALEX stations (Barbosa, Cid Almeida and Montante platform). Their coordinates were used to locate corresponding grid points on the C domain output. In the case of land stations with grid point associated to water fraction, the nearest land grid point was chosen.

5   Figure 6 shows the time evolution of simulated and observed air temperature and wind speed at Cid Almeida, Barbosa, and Montante sites. Overall, the simulation results are slightly more conservative (except wind speed over the Montante platform), but in general, the patterns are well represented. The model could not represent well the maximum and minimum temperatures, especially in land stations where the temperature range is larger. Regarding wind speed, the model underestimates the maximum values at land stations and at Montante platform (Fig. 6 (d)), on the contrary, the wind speed is overestimated by the model,

10   but the principal features of the curve is represented. Statistical values for this validation are the following. For Barbosa: air temperature average bias is 0.23 °C, RMSE is 1.37 °C and correlation coefficient is 0.98, for wind speed these values are: average bias is 0.55 m/s, RMSE is 1.08 m/s, and correlation coefficient is 0.73. For Cid Almeida: temperature average bias is 0.5 °C, RMSE is 1.57 °C, and correlation coefficient is 0.98, wind speed average bias is -0.36 m/s, RMSE is 1.24 m/s, and correlation coefficient is 0.69. For Montante platform: air temperature average bias is -0.1 °C, RMSE is 1.22 °C, correlation is

15   0.98, wind speed average bias is -0.97 m/s, RMSE is 1.55 m/s, and correlation coefficient is 0.61.

The temporal evolution of simulated and observed latent and sensible heat fluxes at Montante platform is shown in Fig. 7 (a, b). Overall patterns of the curves are similar but the simulated one is more smooth. Comparison between measurements and simulated results demonstrates that for latent heat the RMSE is 57.34 Wm^{-2} with correlation coefficient of 0.47, and for sensible heat the RMSE is 13.39 Wm^{-2} with the correlation of 0.82.
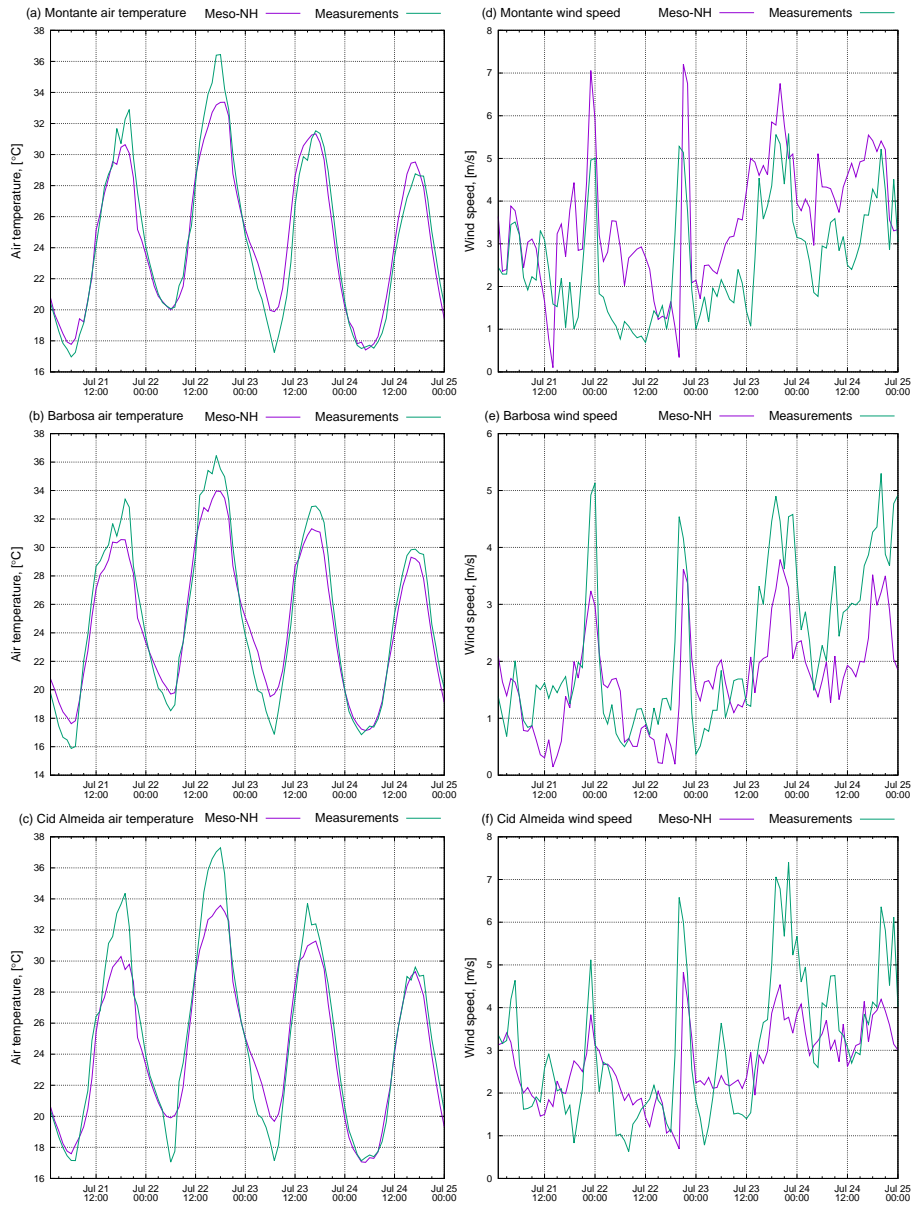
Figure 6. Observed and simulated air temperature and wind speed at 2 meters for ALEX stations: Montante platform (a, d), Barbosa (b, e), and Cid Almeida (c, f) sites.

Both observed and simulated curves of Fig. 7 (a) reveal that sensible heat flux has two different periods during the day, positive when air-water temperature difference is negative, and vice-versa, showing that during daytime the water gets energy from the air and during night-time the water warms the nearby air. The transition between the two regimes is well captured by the model. Fig. 7 (b) also shows that the magnitude of the sensible heat flux is relatively small when compared with the other
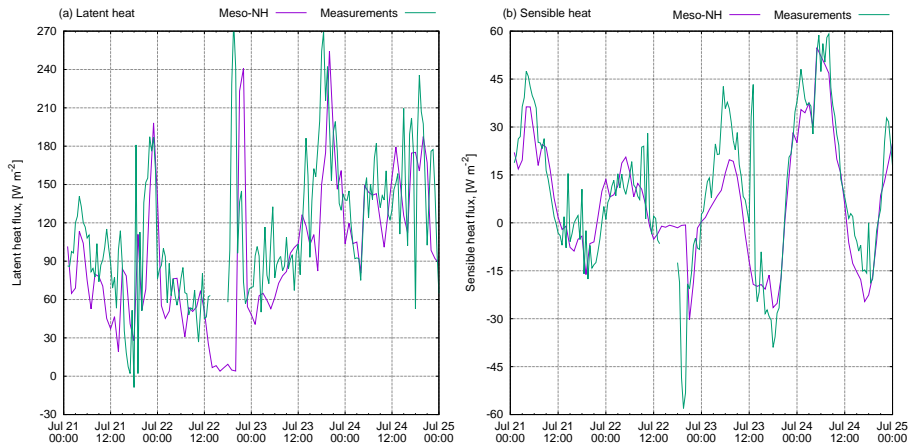
Figure 7. Observed and simulated latent (a) and sensible (b) heat fluxes at Montante floating platform.

terms of the energy balance. Daily maximum positive (negative) fluxes between 30 and 60 $\mathrm{Wm^{-2}}$ (-15 and -30 $\mathrm{Wm^{-2}}$) are well reproduced by the model. An apparently strange behavior appears on July 22 afternoon, with the sensible heat flux being almost zero. This effect, unfortunately not documented due to the lack of data, will be discussed later and is linked to the fact that the wind is very weak during this period (see Fig. 6 (d)).

5   More detailed analysis of Fig 7 (a) shows that the lowest heat flux values usually occur during the afternoon (12:00 – 18:00 UTC), under windless conditions, and high peaks in the early evening (20:00 – 21:00 UTC). The simulation reproduces these peaks with 1-2 hour delay which are related to the delay on the simulated wind speed. The magnitude of the latent heat flux daily maximum (order of $200 - 250\ \mathrm{Wm^{-2}}$) is well captured by the model. The delay in the simulation of the peaks reduces the value of the correlation coefficient and is a manifestation of the so-called double-penalty that penalize high-resolution model

10   scores. As seen in the Fig. 7 (b) the simulated latent heat flux is almost zero between 14:00 and 16:00 UTC of July 22. As pointed before, there is a gap in the measurements of the flux during this period, but data from the day before indicates that the results are realistic. This effect of almost zero evaporation from water on a very hot day is contrary to common sense and will be discussed later.

Wind direction at ALEX stations is represented in Fig. 8. Different behaviour in wind direction between the two station from

15   21 to 23 of July is clearly seen from measurements data (green dots). In Barbosa station the wind changes from northwest to south regime during daytime while in Cid Almeida this effect is not observed. In the simulations this difference is not so clear, but is still visible during the afternoon on July 22. Barbosa station, located on the northwest shore of the lake, indicates the presence of the lake breeze because its direction is the opposite to the dominant wind. However, at Cid Almeida station on the southeast shore breeze is co-directed with the dominant wind in the area, so, its appearance is difficult to track.
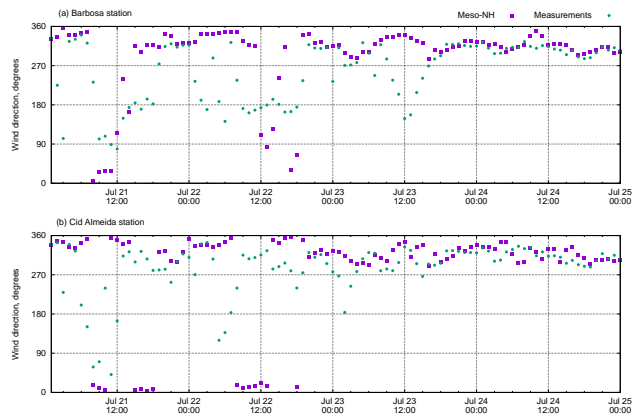
Figure 8. Observed and simulated wind direction on Barbosa and Cid Almeida stations.

6 Lake impact

To analyse the impact of the Alqueva reservoir on local area the changes of the following atmospheric variables, such as air temperature and potential temperature, relative humidity and water mixing ratio, and vertical and horizontal wind speed, were considered. In this section only B and C domain datasets were used.

6.1 Impact on air temperature and relative humidity

The lower layers of air are the first to be affected by the presence of water. Differences in air temperature at 2 meters during 22 July are shown in Fig. 9, the warmest day of the IOP and the one when the breeze was stronger. Positive anomaly (up to 3-4 °C) can be traced during the period from 1 hour after the sunset (21:00 UTC) to 1 hour after the sunrise (07:00 UTC). By positive and negative anomalies here we mean the differences between LAKE1 and LAKE0 simulations. Examples of the positive night anomalies are illustrated in Fig. 9 (a, b). Night northwest wind transports warm air from the lake to the southeast part of the reservoir for up to 2 km away from the shore. Daytime period is characterized by the negative temperature anomaly up to 7 °C (Fig. 9 (c-f)). This effect is essentially limited by the lake borders. When the large-scale sea breeze system arrives, temperature trace of the lake impact is advected by the wind and can be found in 10-12 km away from the southeast part of the reservoir (Fig. 9 (f)).

Vertical cross-sections help to illustrate the processes in the atmosphere on different altitudes. Two different cross-sections S1 and S2 (the first one crosses the lake near Montante platform and the second in the middle, exact locations are indicated in Fig. 9, (a)) are shown to provide a better visualization of the three-dimensional structure of air circulation above the lake. Cross-sections S1 along 38.215 °N (Fig. 10) show the evolution of wind and the potential temperature during the 22 July in the experiment with the reservoir (simulation LAKE1). The highest impact on the air temperature can be observed in the early afternoon (12:00 – 14:00 UTC). The boundary layer is cooling down and its height decreases from more than 2 km above the land outside to values close to 1 km over the lake surface (Fig. 10 (a)). The thermal anomaly induced by the presence of the reservoir seems to affect an area greater than what was identified at the surface, especially in the middle of the boundary layer. Later on, at 19:00 – 20:00 UTC the powerful ocean breeze system reaches the area and cools the lower (1 km) layer of air by 6-7 K. The progression of the sea breeze front is impressively well shown in Fig. 10 (d) (20:00 UTC), when it reaches the border of the reservoir, and in Fig. 10 (e), (f) (21:00 - 22:00 UTC), when it is already beyond the east bank of the Alqueva reservoir.

Alqueva causes a similar anomaly on 2 m relative humidity which is shown in Fig. 11. At night when the temperature impact is negative some small negative differences in relative humidity can be seen over the lake surface (Fig. 11 (a)). There are also traces of daytime positive impact, essentially due to the decrease of air temperature, advected by the sea breeze in the southeast direction. In the morning, however, the difference of relative humidity can not be detected because the thermal impact is not strong enough (Fig. 11 (b)). Figures 11 (c), (d), and (e) show how relative humidity increases during the daytime over the water surface. The peak of the difference can reach 50% in the afternoon (Fig. 11 (f)). In general, lake impact on relative humidity is limited by the area of the reservoir and does not spread over the surrounding land.
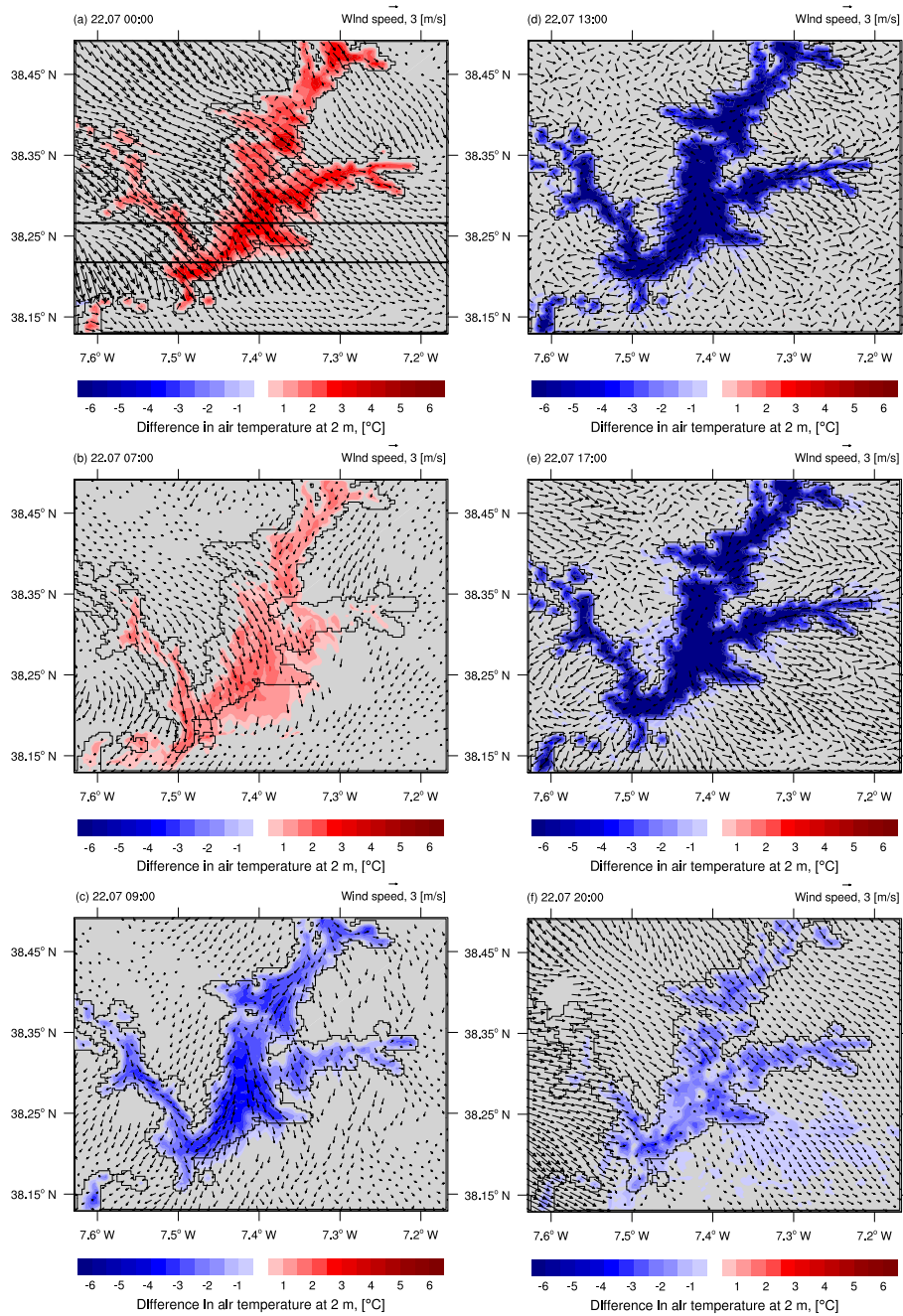
Figure 9. Anomalies in air temperature at 2 m (in filled contours) and horizontal wind in LAKE1 experiment (arrays, the scale is indicated in the upper rigth corner of each figure) of the reservoir on 22 of July 2014 on domain C. Horizontal lines on (a) indicate the location of cross-sections S1 (southern) and S2 (northern).
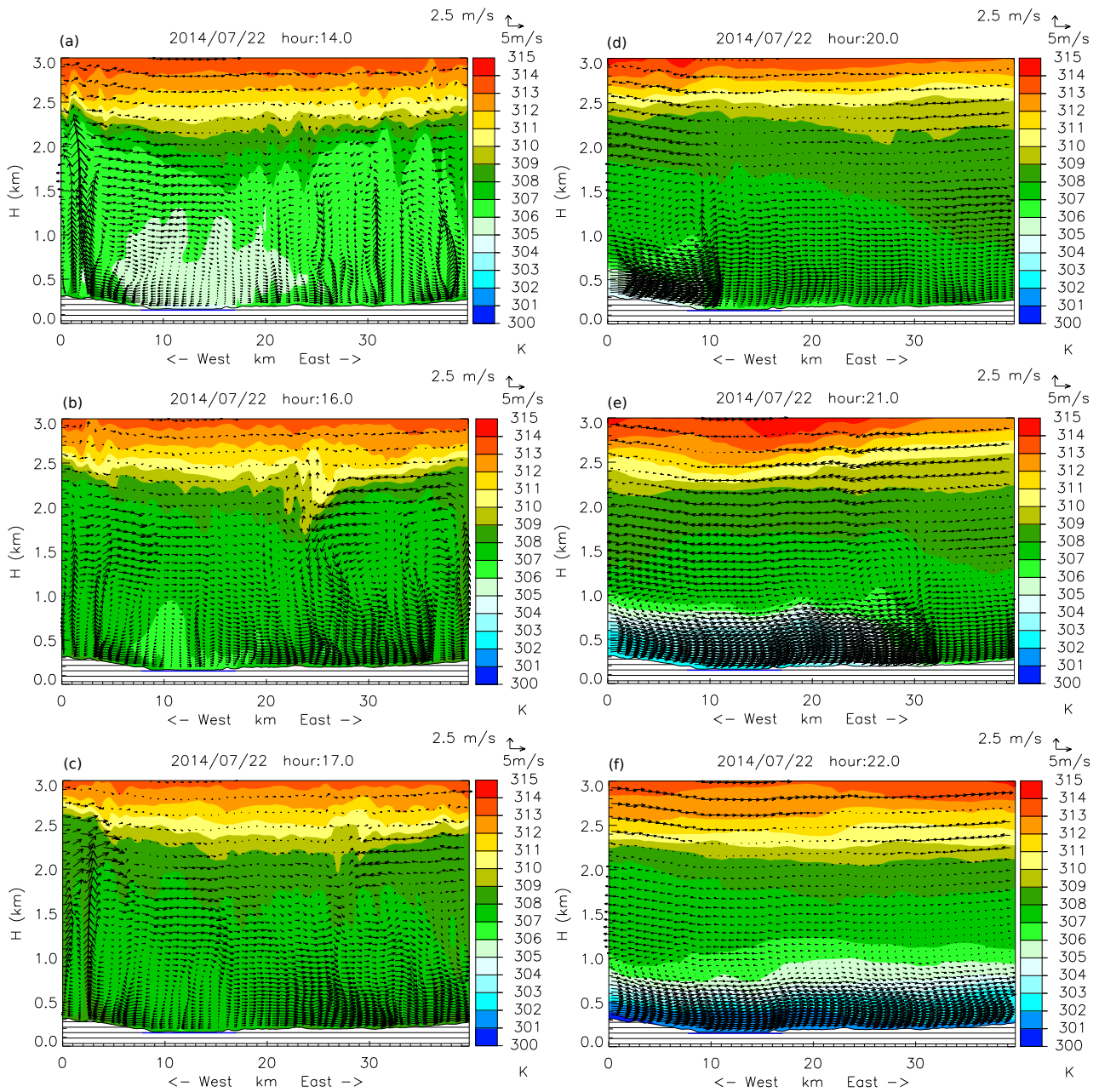
Figure 10. East-west direction cross-sectons along 38.215 °N (S1, crosses the lake near Montante platform, Fig. 9 (a)) of potential temperature (filled contours) and wind vectors in the plane of the cross-section (arrows), at different hours (indicated in the top of each figure) in LAKE1 experiment at 250 m horizontal resolution. The wind vertical and horizontal scales are indicated in the upper right corner of each figure. Blue line on the surface level indicates the location of the reservoir.
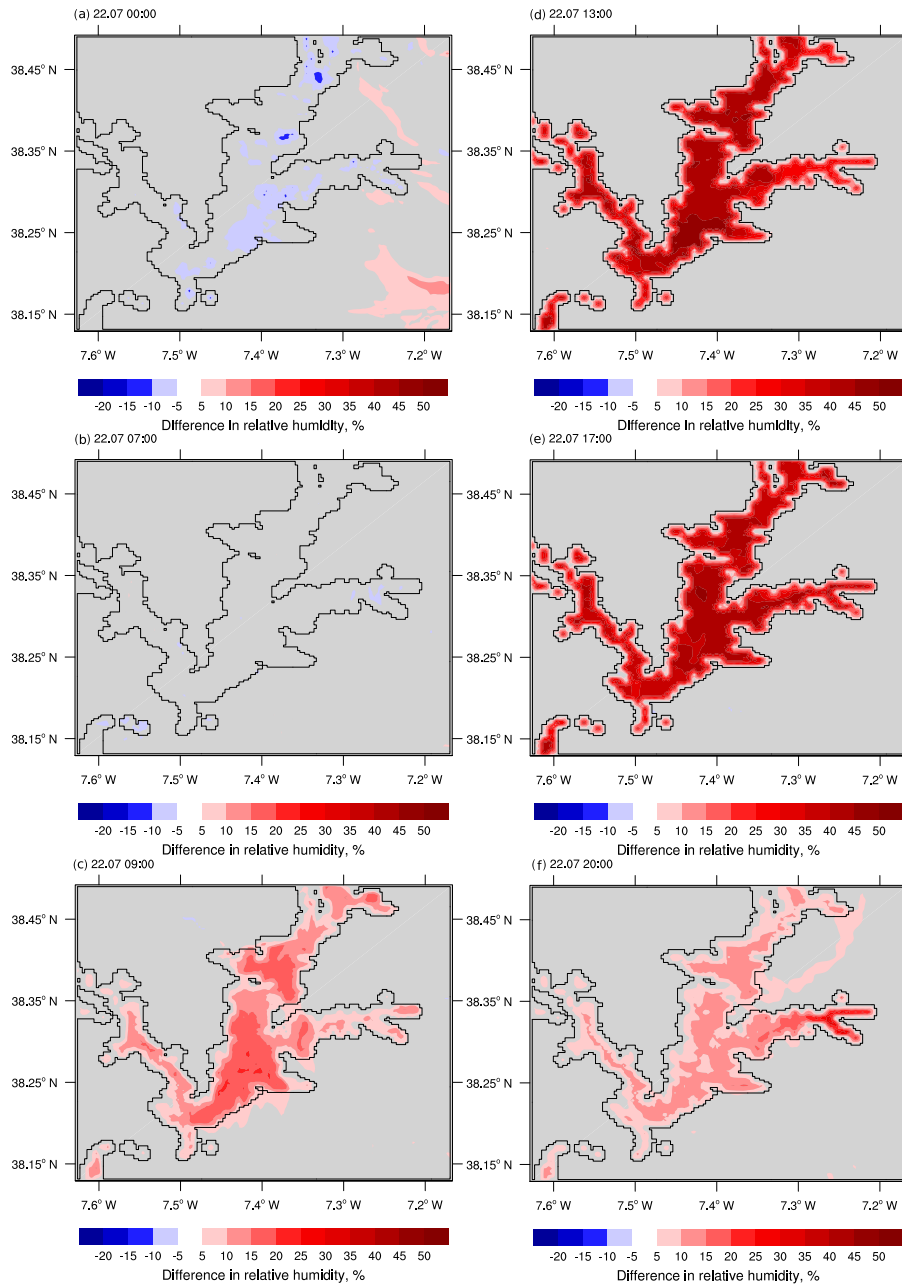
Figure 11. 2 m relative humidity anomalies (in filled contours) on 22 of July 2014 on domain C.

6.2 Breeze effects

Differences in near surface sensible heat fluxes and contrast of the air temperature over the land and water surfaces during the daytime induce the formation of the lake breeze system. The development of the lake breeze is illustrated in Fig. 9 (arrows that

corresponds to the wind speed lesser than 0.5 m/s are not plotted). During the night, the large-scale circulation (Fig. 9 (a), (b)) is dominant in the area. After the sunrise (07:00 – 08:00 UTC) the air temperature over the water surface becomes lower than the air temperature over the surrounding areas, which induce a thermal circulation directed from the center of the lake to its shores. The breeze intensifies during the afternoon reaching 6 m/s in some areas (Fig 9 (d), (e)).

5   Daytime cross-sections S1 in Fig. 10 (a, b, c) indicates that the direct lake breeze can be found on altitudes up to 300 meters above the lake, with a divergent flow over the water surface. The lake breeze intensity and pattern depends on the local orography, but usually the traces can be found 4-6 km away from the lake shores (Fig. 10 (c)). In altitude, a return flow is visible in the eastward wind component over the west shore and a westward component in the east of the reservoir which causes an upper-level convergence which can be seen in Fig. 10 (a, b, c). We will return to this features later together with the

10   discussion of the effects of the reservoir on the moisture field, in which the structure of the lake breeze system is more visible.

In the late afternoon (18:00 UTC) the negative temperature anomaly due to the presence of the lake is getting weaker, and breeze system starts to wane and dissipate. At 19:00 – 20:00 the ocean breeze arrives to the area and overlaps the local circulations (Fig. 10 (d, e, f)).

Cross-sections S1 and S2 presented in Fig. 12 show that the lake breeze system includes a descending branch over the

15   reservoir that carries dry air from a height of about 2-2.5 km and redistribute it over the lake surface. This dry downstream is confirmed by the measurements of water vapor mixing ratio at the Montante platform. As can be seen in Fig. 13 the observed and the simulated mixing ratio of water vapor have a daily minimum with average values of about 8-8.5 g kg^{-1} around 14:00-16:00. During the afternoon of July 22, the day with a strong lake breeze, the minimum reached a value lower than 6 g kg^{-1}. Out of the period in which the air over the lake subsides, the water vapor mixing ratio returns beck to 9-10.5 g kg^{-1}.

20   The presence of this dry downstream was proposed as a hypothesis by Potes et al. (2017) and is proved through the performed simulations. In the same Fig. 13 it is clearly seen that the model tends to overestimating the mixing ratio, except in the afternoon of July 22.

On the other hand, Fig. 12 also shows that outside the reservoir there are zones of low-level convergence and upward motion that increase the moisture of the boundary layer and form some kind of lake breeze fronts. The complex shape of the reservoir

25   implies an also complex 3D structure of the breeze system. Towards the southernmost part, near the dam, the low level divergent breeze circulation is very clear, but the convergence upper-level return current is weaker (Fig. 12 (a, b, c)). In contrary, near the middle of the reservoir (cross-section S2 in Fig. 12 (d, e, f)) where two water branches exist, the circulation near the surface is more complex due to the presence of a land area inbetween, but the subsidence motion is more prominent, inducing a decrease in mixing ratio through the boundary layer, which reaches a magnitude of about 4 g kg^{-1} at 16:00 (Fig. 12 (f)).

30   Figure 14 illustrates this process in a horizontal plane. At midnight (Fig 14 (b)) the reservoir does not directly affect vapour mixing ratio in the air. In the morning hours, when the sun has risen, but the breeze system has not yet formed, a positive impact on the moisture over the lake can be seen due to the increase of the evaporation. This anomaly affects the air above central and southern part of the reservoir and is advected to other nearby areas (Fig 14 (c)). Later in the afternoon, with the formation of the lake breeze, a negative impact can be traced over the water surface due to the descending branches of the local

35   circulation (Fig. 14 (d, e)). This explains the afternoon decrease of the water vapour mixing ratio observed at the Montante
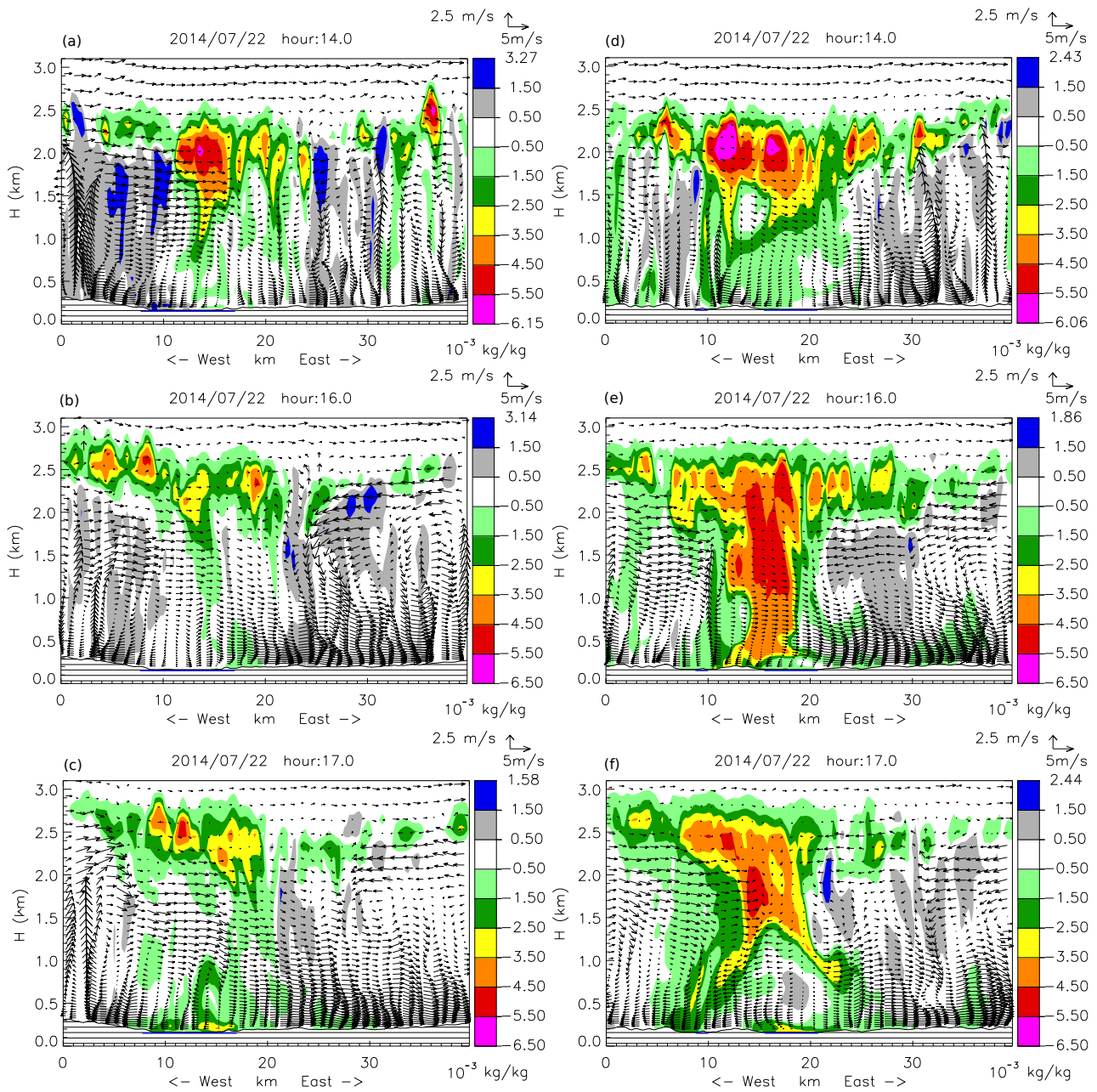
Figure 12. East-west direction cross-sections S1 along 38.215 °N (a,b,c) and S2 along 38.274 °N (d, e, f) with the difference (LAKE1 and LAKE0 simulations) of water mixing ratio (filled contours), and wind vectors in the plane of the cross-section (arrows) in LAKE1 experiment at 250 m horizontal resolution at different times (indicated in the top of each figure). Blue line on the surface level indicates the location of the reservoir.
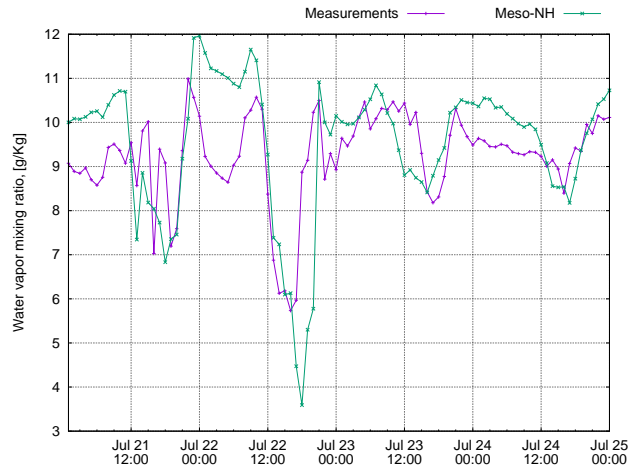
Figure 13. Observed and simulated water vapor mixing ratio over the Montante platform.

platform as seen in Fig 13. The localization of the area of this negative anomaly changes in time, but predominantly it is over the larger southern part of the reservoir. With the dissipation of the local lake breeze system and the arriving of the stronger large scale northwestern wind, the negative moisture anomaly over the reservoir disappears and a positive effect is visible on the downwind region (Fig. 14 (a, f)), due to the increase of evaporation (note that Fig. 14 (a) corresponds to the night of July
5   21 to 22, when the effect was more noticeable).

During daytime, the water temperature is lower than the air temperature, which is associated to a very weak air circulation over the water surface which leads to very low evaporation from the lake (refer to low latent heat flux values in Fig. 7 (a)). At this time period evaporation over the land is even higher that over the water. By late afternoon when the dominant sea breeze system reaches the region, the northwestern wind accelerates significantly, passing over the smooth surface of the lake. As
10 result, evaporation from the lake becomes very intense.

7   Conclusions

This work is dedicated to the studies of the formation and magnitude of the summer lake breeze at the Alqueva reservoir, South Portugal, one of the impacts of the artificial lake on the local weather. The study was based on Meso-NH simulations of a well documented case study of 22-24 July 2014. This period was taken for several reasons. First, a large volume of meteorological
15 data was collected during these days, which allowed for a validation of the simulation results. Secondly, this period was hot and dry, which is typical for most summer days in this region.

The model allowed to conduct the simulation with horizontal resolution of 250 meters which is fine enough to resolve such relatively small scale lake breeze and to spot the impact of the reservoir on the detailed local boundary layer structure. Due to the "youth" of the Alqueva reservoir it is possible to run atmospheric model with the surface conditions prevailing before the
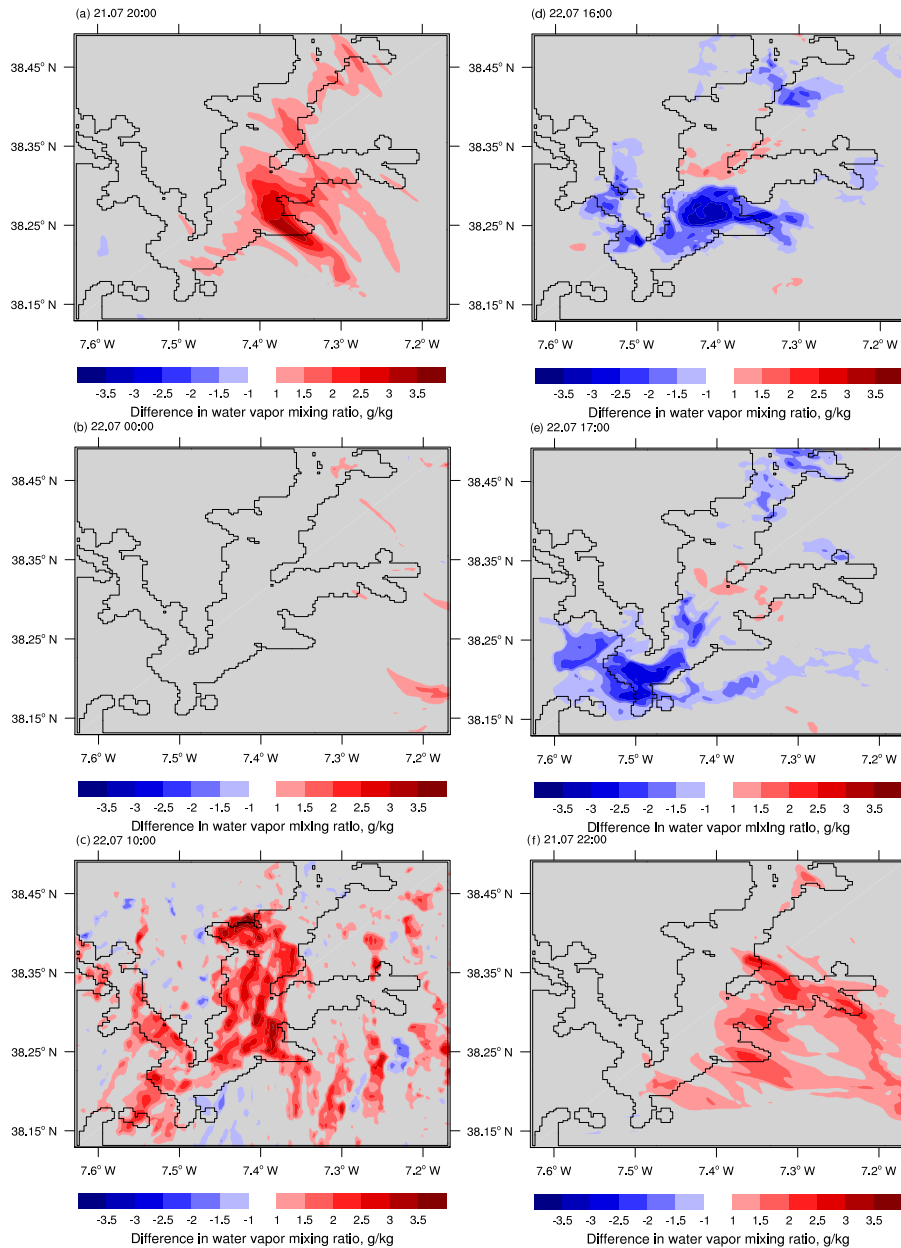
Figure 14. Observed and simulated water vapor mixing ratio anomalies in filled contours on 22 of July 2014 on domain C for selected hours

filling of the reservoir. Two simulations, one with Alqueva and another one without it, allow to evaluate the raw impact of the lake on the local weather regime.

Formation and dissipation of the daytime breeze system induced by the reservoir are described in the work. On hot summer mornings the difference between air temperatures above water and neighbouring land surfaces induces the radial movement

of air from the lake. The breeze system starts to form in the morning and the peak of the wind speed reaches 6 m/s in the late afternoon. Simulation results show that the lake breeze could be detected at a distance of more than 6 km away from the the shores and on altitudes up to 300 m above water surface. In late afternoon the dissipation stage of the lake breeze system anticipated with the arrival of the larger scale sea breeze from the Portuguese west Atlantic coast. In early evening (19:00 –

5   20:00 UTC) the local lake breeze system can not be detected anymore. No reverse land breeze is detected during the night.

During daytime, the simulation testify the observed very low evaporation from water surface (0 – 120 Wm^{-2} in terms of sensible heat flux), due to weak winds and the stable stratification of the internal atmospheric surface layer. A night-time, the strong winds associated with the Peninsular larger-scale circulation induced by the sea-land contrasts, induce a very high evaporation rate (200 – 250 Wm^{-2}).

10 The cooling effect of the reservoir can decrease the air temperature up to 7 °C, nevertheless is limited by the lake borders and normally can not be seen farther than few kilometers away from the shore mostly in southeast direction. The cooling can be found up to 1200 m above the lake surface.

Lake breeze system brings dry air from upper atmospheric layers (2-2.5 km) to near surface levels above the reservoir. This effect leads to the fact that the air above the surface of the lake becomes more dry in terms of water vapor mixing ratio, in spite

15 of its relative humidity can increase up to 50% due to the decrease in air temperature.

Further work implies two directions. The first is tuning the lake model and its initialization in order to obtain more accurate results and reduce validation biases. The second is to carry out a longer experiment, which would cover a 12-month period. Such simulation could reveal seasonal aspects of the impact of Alqueva on local weather.

Competing interests. The authors declare that they have no conflict of interest.

20 *Acknowledgements.* The work is co-funded by the European Union through the European Regional Development Fund, included in the COMPETE 2020 (Operational Program Competitiveness and Internationalization) through the ICT project (UID / GEO / 04683/2013) with the reference POCI-01-0145-FEDER-007690 and also through the ALOP project (ALT20-03-0145-FEDER-000004). Experiments were accomplished during the field campaign funded by FCT and FEDER-COMPETE: ALEX (EXPL/GEO-MET/1422/2013) FCOMP-01-0124-FEDER-041840.

References

Bates, G. T., Giorgi, F., and Hostetler, S. W.: Toward the Simulation of the Effects of the Great Lakes on Regional Climate, Monthly Weather Review, 121, 1373–1387, https://doi.org/10.1175/1520-0493(1993)121<1373:TTSOTE>2.0.CO;2, 1993.

Bechtold, P., Bazile, E., Guichard, F., Mascart, P., and Richard, E.: A mass-flux convection scheme for regional and global models, Quarterly Journal of the Royal Meteorological Society, 127, 869–886, https://doi.org/10.1002/qj.49712757309, 2001.

Bischoff-Gauß, I., Kalthoff, N., and Fiebig-Wittmaack, M.: The influence of a storage lake in the Arid Elqui Valley in Chile on local climate, Theoretical and Applied Climatology, 85, 227–241, https://doi.org/10.1007/s00704-005-0190-8, 2006.

Bonan, G. B.: Sensitivity of a GCM Simulation to Inclusion of Inland Water Surfaces, Journal of Climate, 8, 2691–2704, https://doi.org/10.1175/1520-0442(1995)008<2691:SOAGST>2.0.CO;2, 1995.

Bougeault, P. and Lacarrere, P.: Parameterization of Orography-Induced Turbulence in a Mesobeta–Scale Model, Monthly Weather Review, 117, 1872–1890, https://doi.org/10.1175/1520-0493(1989)117<1872:POOITI>2.0.CO;2, 1989.

Cohard, J.-M. and Pinty, J.-P.: A comprehensive two-moment warm microphysical bulk scheme. I: Description and tests, Quarterly Journal of the Royal Meteorological Society, 126, 1815–1842, https://doi.org/10.1002/qj.49712656613, 2000.

Cotton, W. R. and Pielke, R. A. S.: Human Impacts on Weather and Climate, Cambridge University Press, 2nd edn., 2007.

Crosman, E. T. and Horel, J. D.: Idealized Large-Eddy Simulations of Sea and Lake Breezes: Sensitivity to Lake Diameter, Heat Flux and Stability, Boundary-Layer Meteorology, 144, 309–328, https://doi.org/10.1007/s10546-012-9721-x, 2012.

Cuxart, J., Bougeault, P., and Redelsperger, J.-L.: A turbulence scheme allowing for mesoscale and large-eddy simulations, Quarterly Journal of the Royal Meteorological Society, 126, 1–30, https://doi.org/10.1002/qj.49712656202, 2000.

Drobinski, P. and Dubos, T.: Linear breeze scaling: from large-scale land/sea breezes to mesoscale inland breezes, Quarterly Journal of the Royal Meteorological Society, 135, 1766–1775, https://doi.org/10.1002/qj.496, 2009.

Ekhtiari, N., Grossman-Clarke, S., Koch, H., Souza, W. M., Donner, R. V., and Volkholz, J.: Effects of the Lake Sobradinho Reservoir (Northeastern Brazil) on the Regional Climate, Climate, 5, https://doi.org/10.3390/cli5030050, 2017.

Faroux, S., Kaptué Tchuenté, A. T., Roujean, J.-L., Masson, V., Martin, E., and Le Moigne, P.: ECOCLIMAP-II/Europe: a twofold database of ecosystems and surface parameters at 1 km resolution based on satellite information for use in land surface, meteorological and climate models, Geoscientific Model Development, 6, 563–582, https://doi.org/10.5194/gmd-6-563-2013, 2013.

Fouquart, Y. and Bonnel, B.: Computations of Solar Heating of the Earth's Atmosphere — A New Parameterization., Beitrage zur Physik der Atmosphare, 53, 35–62, 1980.

Hartmann, D. L.: Global physical climatology, International geophysics, 1994.

Hoinka, K. P. and Castro, M. D.: The Iberian Peninsula thermal low, Q. J. Roy. Meteorol. Soc., 129(590), 1491–1511, 2003.

Jarvis, A., Guevara, E., Reuter, H. I., , and Nelson, A. D.: Hole - filled SRTM for the globe : version 4 : data grid, published by CGIAR-CSI on 19 August 2008., 2008.

Kain, J. S. and Fritsch, M. J.: A One-Dimensional Entraining/Detraining Plume Model and Its Application in Convective Parameterization, Journal of the Atmospheric Sciences, 47, 2784–2802, https://doi.org/10.1175/1520-0469(1990)047<2784:AODEPM>2.0.CO;2, 1990.

Lac, C., Chaboureau, J.-P., Masson, V., Pinty, J.-P., Tulet, P., Escobar, J., Leriche, M., Barthe, C., Aouizerats, B., Augros, C., Aumond, P., Auguste, F., Bechtold, P., Berthet, S., Bielli, S., Bosseur, F., Caumont, O., Cohard, J.-M., Colin, J., Couvreux, F., Cuxart, J., Delautier, G., Dauhut, T., Ducrocq, V., Filippi, J.-B., Gazen, D., Geoffroy, O., Gheusi, F., Honnert, R., Lafore, J.-P., Lebeaupin Brossier, C., Libois, Q., Lunet, T., Mari, C., Maric, T., Mascart, P., Mogé, M., Molinié, G., Nuissier, O., Pantillon, F., Peyrillé, P., Pergaud, J., Perraud, E., Pianezze,

J., Redelsperger, J.-L., Ricard, D., Richard, E., Riette, S., Rodier, Q., Schoetter, R., Seyfried, L., Stein, J., Suhre, K., Thouron, O., Turner, S., Verrelle, A., Vié, B., Visentin, F., Vionnet, V., and Wautelet, P.: Overview of the Meso-NH model version 5.4 and its applications, Geoscientific Model Development Discussions, 2018, 1–66, https://doi.org/10.5194/gmd-2017-297, 2018.

Lascaux, F., Masciadri, E., and Fini, L.: MOSE: operational forecast of the optical turbulence and atmospheric parameters at European Southern Observatory ground-based sites — II. Atmospheric parameters in the surface layer 0-30 m, Monthly Notices of the Royal Astronomical Society, 436, 3147–3166, https://doi.org/10.1093/mnras/stt1803, 2013.

Lascaux, F., Masciadri, E., and Fini, L.: Forecast of surface layer meteorological parameters at Cerro Paranal with a mesoscale atmospherical model, Monthly Notices of the Royal Astronomical Society, 449, 1664–1678, https://doi.org/10.1093/mnras/stv332, 2015.

Lee, X., Liu, S., Xiao, W., Wang, W., Gao, Z., Cao, C., Hu, C., Hu, Z., Shen, S., Wang, Y., Wen, X., Xiao, Q., Xu, J., Yang, J., and Zhang, M.: The Taihu Eddy Flux Network: An Observational Program on Energy, Water, and Greenhouse Gas Fluxes of a Large Freshwater Lake, Bulletin of the American Meteorological Society, 95, 1583–1594, https://doi.org/10.1175/BAMS-D-13-00136.1, 2014.

Lopes, F., Silva, H. G., Salgado, R., Potes, M., Nicoll, K. A., and Harrison, R. G.: Atmospheric electrical field measurements near a fresh water reservoir and the formation of the lake breeze, Tellus A: Dynamic Meteorology and Oceanography, 68, 31 592, https://doi.org/10.3402/tellusa.v68.31592, 2016.

Lunet, L., Lac, C., Auguste, F., Visentin, F., Masson, V., and Escobar, J.: Combination of WENO and Explicit Runge–Kutta Methods for Wind Transport in the Meso-NH Model, Monthly Weather Review, 145, 3817–3838, https://doi.org/10.1175/MWR-D-16-0343.1, 2017.

Masciadri, E., Lascaux, F., and Fini, L.: MOSE: operational forecast of the optical turbulence and atmospheric parameters at European Southern Observatory ground-based sites — I. Overview and vertical stratification of atmospheric parameters at 0-20 km, Monthly Notices of the Royal Astronomical Society, 436, 1968–1985, https://doi.org/10.1093/mnras/stt1708, 2013.

Masson, V.: A Physically-Based Scheme For The Urban Energy Budget In Atmospheric Models, Boundary-Layer Meteorology, 94, 357–397, https://doi.org/10.1023/A:1002463829265, 2000.

Masson, V., Le Moigne, P., Martin, E., Faroux, S., Alias, A., Alkama, R., Belamari, S., Barbu, A., Boone, A., Bouyssel, F., Brousseau, P., Brun, E., Calvet, J.-C., Carrer, D., Decharme, B., Delire, C., Donier, S., Essaouini, K., Gibelin, A.-L., Giordani, H., Habets, F., Jidane, M., Kerdraon, G., Kourzeneva, E., Lafaysse, M., Lafont, S., Lebeaupin Brossier, C., Lemonsu, A., Mahfouf, J.-F., Marguinaud, P., Mokhtari, M., Morin, S., Pigeon, G., Salgado, R., Seity, Y., Taillefer, F., Tanguy, G., Tulet, P., Vincendon, B., Vionnet, V., and Voldoire, A.: The SURFEXv7.2 land and ocean surface platform for coupled or offline simulation of earth surface variables and fluxes, Geoscientific Model Development, 6, 929–960, https://doi.org/10.5194/gmd-6-929-2013, 2013.

Miranda, P., Abreu, F., and Salgado, R.: Estudo de Impacte Ambiental do Alqueva, Tech. rep., Instituto de ciencia aplicada e tecnologia, Faculdade de Ciências, Universidade de Lisboa, 1995.

Miranda, P. M. and James, I. N.: Non-linear three-dimensional effects on gravity-wave drag: Splitting flow and breaking waves, Quarterly J. Royal Meteorological Society, 118, 1057–1081, 1992.

Mironov, D.: Parameterization of lakes in numerical weather prediction. Description of a lake model. COSMO Technical Report, Deutscher Wetterdienst, 11, Pp. 41, 2008.

Morcrette, J.-J.: Radiation and cloud radiative properties in the European Centre for Medium Range Weather Forecasts forecasting system, Journal of Geophysical Research: Atmospheres, 96, 9121–9132, https://doi.org/10.1029/89JD01597, 1991.

Nicoll, K. A., Harrison, R. G., Silva, H. G., Salgado, R., Melgâo, M., and Bortoli, D.: Electrical sensing of the dynamical structure of the planetary boundary layer, Atmospheric Research, 202, 81–95, https://doi.org/https://doi.org/10.1016/j.atmosres.2017.11.009, 2018.

Noilhan, J. and Mahfouf, J.-F.: The ISBA land surface parameterisation scheme, Global and Planetary Change, 13, 145 – 159, https://doi.org/10.1016/0921-8181(95)00043-7, soil Moisture Simulation, 1996.

Pergaud, J., Masson, V., Malardel, S., and Couvreux, F.: A Parameterization of Dry Thermals and Shallow Cumuli for Mesoscale Numerical Weather Prediction, Boundary-Layer Meteorology, 132, 83, https://doi.org/10.1007/s10546-009-9388-0, 2009.

5 Pielke, R. A.: A Three-Dimensional Numerical Model of the Sea Breezes Over South Florida, Monthly Weather Review, 102, 115–139, https://doi.org/10.1175/1520-0493(1974)102<0115:ATDNMO>2.0.CO;2, 1974.

Pielke, R. A. S.: Mesoscale Meteorological Modeling, Academic Press, 3rd edn., 2013.

Pinty, J.-P. and Jabouille, P.: A mixed-phase cloud parameterization for use in mesoscale non-hydrostatic model: simulations of a squall line and of orographic precipitations., Proc. Conf. of Cloud Physics, Everett, WA, USA, Amer. Meteor. soc., pp. 217–220, 1998.

10 Policarpo, C., Salgado, R., and ao C., M. J.: Numerical Simulations of Fog Events in Southern Portugal, Advances in Meteorology, 2017, 16, 2017.

Potes, M., Salgado, R., Costa, M. J., Morais, M., Bortoli, D., Kostadinov, I., and Mammarella, I.: Lake–atmosphere interactions at Alqueva reservoir: a case study in the summer of 2014, Tellus A: Dynamic Meteorology and Oceanography, 69, 1272 787, https://doi.org/10.1080/16000870.2016.1272787, 2017.

15 Salgado, R.: Interacção solo-atmosfera em clima semi-àrido, Ph.D. thesis, Universidade de Èvora, 2006.

Salgado, R. and Le Moigne, P.: Coupling of the FLake model to the Surfex externalized surface model, Boreal Environ. Res., 15, 231–244, 2010.

Salgado, R., Miranda, P. M. A., Lacarrère, P., and Noilhan, J.: Boundary layer development and summer circulation in Southern Portugal, Tethys, 12, 33–44, https://doi.org/10.3369/tethys.2015.12.03, 2015.

20 Samuelsson, P., Kourzeneva, E., and Mironov, D.: The impact of lakes on the European climate as simulated by a regional climate model, Boreal Environment Research, 15, 113–129, http://www.borenv.net/BER/pdfs/ber15/ber15-113.pdf, 2006.

Segal, M., Leuthold, M., Arritt, R. W., Anderson, C., and Shen, J.: Small Lake Daytime Breezes: Some Observational and Conceptual Evaluations, Bulletin of the American Meteorological Society, 78, 1135–1147, https://doi.org/10.1175/1520-0477(1997)078<1135:SLDBSO>2.0.CO;2, 1997.

25 Silva, A., De Lima, I., Santo, F., and V., P.: Assessing changes in drought and wetness episodes in drainage basins using the Standardized Precipitation Index, Bodenkultur, 65 (3-4), 31–37, 2014.

Stein, J., Richard, E., Lafore, J. P., Pinty, J. P., Asencio, N., and Cosma, S.: High-Resolution Non-Hydrostatic Simulations of Flash-Flood Episodes with Grid-Nesting and Ice-Phase Parameterization, Meteorology and Atmospheric Physics, 72, 203–221, https://doi.org/10.1007/s007030050016, 2000.

30 Thiery, W., Martynov, A., Darchambeau, F., Descy, J.-P., Plisnier, P.-D., Sushama, L., and van Lipzig, N. P. M.: Understanding the performance of the FLake model over two African Great Lakes, Geoscientific Model Development, 7, 317–337, https://doi.org/10.5194/gmd-7-317-2014, 2014.

Zhao, L., Jin, J., Wang, S.-Y., and Ek, M. B.: Integration of remote-sensing data with WRF to improve lake-effect precipitation simulations over the Great Lakes region, Journal of Geophysical Research: Atmospheres, 117, https://doi.org/10.1029/2011JD016979, d09102, 2012.